Activity standardisation of ^{32}Si at IRA-METAS

Youcef Nedjadi [a,*], M. Teresa Durán [a], Frédéric Juget [a], François Bochud [a], Mario Veicht [b],
Dorothea Schumann [b], Ionut Mihalcea [b], Karsten Kossert [c], Claude Bailat [a]

[a] *Institut de Radiophysique, Lausanne, Switzerland*
[b] *Laboratory of Radiochemistry, Paul Scherrer Institut, Villigen-PSI, Switzerland*
[c] *Physikalisch-Technische Bundesanstalt (PTB), Bundesallee 100, 38116, Braunschweig, Germany*

A B S T R A C T

This work explores the primary activity standardisation of ^{32}Si as part of the SINCHRON project that aims at filling the geochronological dating gap by making a new precise measurement of the half-life of this nuclide. The stability of some of the radioactive test solutions, providing ^{32}Si as hexafluorosilicic acid ($H_2^{32}SiF_6$), was monitored over long periods, pointing to the adequate sample composition and vial type to ensure stability. These solutions were standardised using liquid scintillation counting with the triple to double coincidence ratio (TDCR) technique and the CIEMAT-NIST efficiency tracing (CNET) method. Complementary backup measurements, using $4\pi\beta$-γ coincidence counting with ^{60}Co as a tracer, were performed with both liquid and plastic scintillation for beta detection. While ^{60}Co coincidence tracing with a liquid scintillator predicted activities in agreement with the TDCR and CNET determinations, using plastic scintillation turned out to be unfeasible as the addition of lanthanum nitrate and ammonia to fix the silicon during the drying process generated large crystals that compromised the linearity of the efficiency function.

1. Introduction

Radioisotope dating is used in geochronology to establish the absolute geologic age of samples. Silicon-32, a pure beta emitter and a natural isotope of silicon produced in the atmosphere from cosmic spallation of Argon, has a half-life of about 150 years which fills the prevailing dating gap between chronologies determined through ^{210}Pb (22.23(12) year half-life) and ^{14}C (5700(30) year half-life) (Lal et al., 1976; Tykva and Berg, 2004; Aggarwal et al., 2007; Veicht et al., 2021; Veicht, 2022). This is a key motivation behind the SINCHRON project, recently set up to make a new precise determination of the ^{32}Si half-life.

Earlier measurements of this half-life were made with low activity ^{32}Si sources (Fifield and Morgenstern, 2009). In this project, ^{32}Si was produced through high-energy proton irradiation of metallic vanadium discs at the Paul Scherrer Institut (PSI). Ion-exchange, extraction and chelating chromatography were combined to produce a pure ^{32}Si solution (Veicht et al., 2021).

As part of the SINCHRON collaboration, IRA-METAS, the Swiss designated metrological institute for radioactivity, along with the PTB, were tasked with determining the activity concentration of the pure ^{32}Si solution, while the measurements of the number of ^{32}Si atoms using

mass spectrometry were performed by other partner laboratories in the collaboration.

IRA-METAS received five different solutions of ^{32}Si over a period of three years. The liquid scintillation samples prepared from some of these solutions were monitored for extensive periods to identify sample compositions and vial types conducive to long-term stability. All these solutions were standardised using the TDCR and CNET techniques (Grau Malonda, 1999; Broda et al., 2007). $4\pi\beta$-γ coincidence counting, with ^{60}Co as a tracer (Baerg et al., 1964; Chun Guang Yan et al., 2002), was carried out with both liquid and plastic scintillators in the beta channel to check independently the other liquid scintillation counting methods. ^{60}Co coincidence tracing with a liquid scintillator yielded activities compatible with the TDCR and CNET measurements. However, the same tracing technique with plastic scintillators was inconclusive because the large crystals produced by the source drying procedure led to marked non-linearities in the efficiency function.

These methods for activity standardisation and their main results are described in this paper.

---

* Corresponding author.
  E-mail address: youcef.nedjadi@chuv.ch (Y. Nedjadi).

2. Material and methods

Ion-exchange chromatography was employed to separate the bulk target material (vanadium), and to concurrently eliminate main impurities (e.g., ^{22}Na, ^{44}Ti/^{44}Sc, ^{60}Co, ^{172}Hf, ^{172,173}Lu). In order to provide enhanced purity, an extraction resin (LN® resin, TrisKem, France) and a chelating resin (Monophos®, TrisKem, France) were also used. Consequently, traces of remnant radionuclides were quantitatively removed. Finally, evaporation to dryness removed volatile nuclides, here, tritium and two argon radioisotopes. Following the radiochemical separation procedure, described in detail by Veicht et al. (2021), the final ^{32}Si eluates obtained at PSI and prepared for distribution contain radiosilicon in the form of hexafluorosilicic acid (HSiA, H$_2$SiF$_6$), in a HCl 0.5 mol/L matrix.

2.1. ^{32}Si solutions

PSI sent five different radioactive HSiA solutions to IRA-METAS. The first one, denoted M32Si1, was received in July 2020 in a plastic vial containing about 5 g and 70 kBq of a solution prepared from a single irradiated vanadium disk. Its chemical separation had been made on 9 March 2020, and it had undergone five evaporations to remove tritium residues. This solution was considered part of the method development at PSI, in order to prove that ^{32}Si solutions with the required purity can be provided within the SINCHRON collaboration.

The second solution, M32Si2, was in a plastic vial received in May 2021. It was an about 100 kBq/g aliquot from a solution produced with six irradiated vanadium disks, whereby the fully developed separation procedure was applied. It had been chemically separated on 23 December 2020, and the eluate had been evaporated ten times to eliminate tritium traces. PSI sent us a second aliquot from their stock of the same solution in January 2022 for further tests. Since the radioactive concentration of the solution changed slightly during storage, this second batch is named M32Si6.

Three other solutions, indicated as M32Si3-5 respectively, were received on 29 September 2021. Each of these 5 g aliquots in Eppendorf vials came from one different vanadium disk. Their mother solutions had all been chemically separated in parallel on 14 July 2021. Subsequently, M32Si3-5 underwent 10, 30 and 50 evaporations, respectively, to remove potential tritium remnants.

2.2. Sources

2.2.1. Liquid scintillation sources

To perform TDCR and CNET measurements from the M32Si1 solution, aliquots from it were dispensed gravimetrically, using a pycnometer, into nine high density polyethylene (HDPE) and two sandblasted glass vials using a pycnometer weighed with a Mettler balance traceable to a primary mass standard. These vials were prefilled with 14.5 mL Ultima Gold (UG) cocktail and topped up with variable volumes of HCl 0.5 mol/L to achieve a 6.5% aqueous fraction. This large aqueous fraction was found to be necessary for the stability of samples over extended periods (Nedjadi et al., 2016), while the addition of HCl 0.5 mol/L, instead of typically water, was preferred in order not to interfere with the speciation of the HSiA (Finney et al., 2006), as hydrolysis caused by the addition of water alters the silicon speciation. Aliquots of carbon tetrachloride were added incrementally to six of the HDPE samples to alter the detection efficiency by chemical quenching. After each sample was prepared, the vial was agitated for 2 min with a vortex shaker, and then centrifuged at 15 revolutions per second for 150 s to settle down the liquid on the cap and walls. A compositionally matched blank was also prepared for background subtractions.

For liquid scintillation counting using solutions M32Si2-5, the same protocol was followed. Eleven HDPE vials were gravimetrically prepared using UG and HCl 0.5 mol/L top-ups to achieve a 6.5% aqueous fraction. No glass vial was used. Seven of these samples were quenched

with multiple volumes of carbon tetrachloride.

The same procedure was also used for solution M32Si6, but in this case two additional samples were made without adding any top-up, and two samples were prepared with a water top-up matching in volume the gravimetrically deposited radioactive silicon aliquot.

For the CNET standardisations, two different quenched sets of content-matched UG tritium sources were also composed, using IRA-METAS tritiated-water activity standards.

2.2.2. ^{60}Co coincidence tracing sources

For $4\pi\beta$(LS)-γ coincidence tracing with ^{60}Co, two ^{60}Co sources as well as four mixed ^{32}Si–^{60}Co sources were prepared from an IRA-METAS ^{60}Co standard and M32Si1. The compound sources were designed in such a way as to vary the silicone-cobalt activity ratio. Both the ^{60}Co and mixed sources were in the form of HDPE vials, with 14.5 mL of UG to which complements of 0.5 mol/L HCl were added to make 6.5% aqueous fractions. Vortex shaking homogenises the cobalt and silicone distributions inside the samples. The same procedure was also used for standardising the M32Si6 solution.

Weighed drops of a ^{60}Co standard solution were also deposited onto one plastic scintillator –ultrasonically cleaned beforehand – for $4\pi\beta$(PS)-γ coincidence measurements. This UPS-923A plastic scintillator is made of two pieces which fit together to form a 25 mm height and 25 mm diameter cylinder, inside which there is a centred cylindrical cavity (3 mm x 12 mm) housing the radioactive deposit. Drops of Ludox colloidal silica (Sigma-Aldrich GmbH, Germany) with a concentration of 0.03% mass fraction were subsequently added to the deposition for homogenising the crystallisation process when drying. After drying, the top and bottom plastic pieces were glued together with optical cement.

Four mixed ^{32}Si–^{60}Co plastic scintillation sources were prepared from the same cobalt solution and M32Si2, with various silicone-cobalt activity ratios, using the same procedure, except that here specific amounts of lanthanum nitrate (La(NO$_3$)$_3$) and ammonium hydroxide (NH$_4$OH) had to be pipetted on top of the radioactive deposits. This procedure, developed at PSI, enabled the drying of the silicon solution without incurring losses, since the HSiA actually releases silicon tetrafluoride (SiF$_4$), a volatile gas. All mixed sources were prepared by combining separate cobalt and silicon aliquots except one that was prepared from a mixed ^{32}Si–^{60}Co solution. Fig. 1 shows a plastic scintillator with a dried mixed ^{32}Si–^{60}Co source. The drying process made in a fume box was successful as no trace of silicon was detected, thus validating the chemical recipe for preventing silicone volatility during drying.

An additional ^{32}Si plastic scintillation source was conditioned in the same way for measuring the half-life by following the decay.

2.2.3. Gamma spectrometry sources

Aliquots from each of the six ^{32}Si solutions were used to prepare six sources in the form of plastic vials filled with 20 mL of HCl 0.5 mol/L.

2.3. Methods

2.3.1. Liquid scintillation counting

Our TDCR system (Nedjadi et al., 2015) operates with a MAC3-module (Bouchard and Cassette, 2000) with adjustable coincidence resolving time. The TDCR electronic system was tuned for an optimal response for ^{32}Si and ^{32}P. For each PMT, the threshold was set at the valley of the single-electron response. Variation of the double and triple coincidence rates with the coincidence window, for silicon sources, pointed to an optimal resolving time of 100 ns. The deadtime is of an extendable type and was set at 90 µs.

Unquenched sources, prepared as described above, were measured by voltage defocusing varying from 560 V to 340 V in 40 V decrements as well as grey filtering with self-adhesive films of varying optical densities. For the quenching measurement, some of these vials, and those quenched with CCl$_4$, were measured with a constant focusing

Fig. 1. UPS923A plastic scintillator with a crystallised ^{32}Si–^{60}Co deposit. Lanthanum nitrate and ammonium hydroxide were added on top of the liquid silicon and cobalt drops to prevent the volatility of silicon during drying.

voltage set at 560 V.

Each sample is measured in a sequence of twenty repetitions with a total counting time ranging from 600 s to 900 s so that the relative standard deviations of the triple coincidence count rates are lower than 0.1%. Accidental coincidences were taken into account using the formalism of (Dutsov et al., 2020). The observed triple-to-double coincidence ratios varied between 0.97 and 0.98 for defocusing measurements, between 0.91 and 0.98 for chemical quenching, and 0.86 and 0.98 in the case of grey filtering.

As for the CNET measurements, they were performed with a Tricarb 2700 TR counter, which uses a ^{133}Ba source for determining the quench parameter (tSIE). The coincidence window was set at 50 ns whereas the delay before burst, i.e. the duration that the detector delays before looking for additional pulses after the prompt pulse of an event, was set at maximum value (800 ns). Every silicon source measurement cycle was preceded by measuring the quenched tritium sources in the same conditions.

2.3.2. *4πβ(LS)-γ(NaI) coincidence counting*

In this technique (Campion et al., 1960; Baerg et al., 1964), ^{32}Si is standardised by measuring a ^{32}Si–^{60}Co mixed source. Since ^{32}Si, ^{32}P and ^{60}Co involve mainly allowed beta minus transitions, one assumes a linear relationship between the beta efficiencies of these nuclides, so the activity of the mixed source can be determined by extrapolating the β-efficiency to 100%. Knowing the activity concentration of ^{60}Co from an independent coincidence determination, one can infer that of ^{32}Si by subtraction.

Beta-channel detection is achieved with a high diffuse reflectance optical chamber that accommodates the liquid scintillation vial between two facing 2-inch photomultiplier tubes. Only the photomultiplier tube (PMT) with the smallest background noise and best signal/noise ratio was used in this application. Electronic discrimination was used to alter the beta detection efficiency. Underneath the optical chamber, an 82 mm diameter NaI(Tl) detector is positioned. This detection system is housed within a shielded case with five cm-thick lead walls.

Pulse processing in both channels is made with analogue electronics. A custom-built digital coincidence selector is used to vary non-extending deadtimes and set the resolving times. A non-extending deadtime of 29 μs was used to ward off PMT afterpulses or scintillator phosphorescence. Although the ^{60}Co delay spectra between the beta and gamma channel pulses had full width half maxima lower than 20 ns, a wide coincidence window of 1.0 μs was set to ensure the detection of all coincidences.

The beta detection efficiency was altered by low-level discrimination. The counting times ranged from 2 min to 25 min per efficiency

point, according to the gamma setting and discrimination level, for the relative standard deviations of the counting rates to be consistently lower than 0.1%. Each of the ^{60}Co and mixed ^{32}Si–^{60}Co sources were measured at two gamma settings: a threshold at the valley before the low-energy X-ray peak, and a threshold at 661.7 keV.

For standardising the M32Si6 solution, the CAEN DT5725 digitizer along with the digital pulse processing for pulse height analysis (DPP-PHA) software were used to shape the pulses. An off-line analysis of the data was made with an in-house code that implements the pulse-mixing method (Bouchard and Chauvenet, 1999).

2.3.3. *4πβ(PS)-4πγ(NaI) coincidence counting*

Here the beta detector is a UPS-923A plastic scintillator optically coupled to a low-noise one-inch diameter photomultiplier tube. The very thin light-tight case that houses this beta detector stands upright at the bottom of the well of a 120 mm x 120 mm NaI(Tl) gamma detector. This system rests at the bottom of a 50-cm-diameter 5-cm-thick cylindrical lead shielding covered with an armour-plated sliding square six cm-thick.

Analogue pulse processing is used as described in 2.3.2. The non-extending deadtime and resolving time were 29 μs and 1 μs, respectively. Electronic discrimination is used to vary the beta detection efficiency. Measurement times per efficiency point varied between 3 and 30 min to ensure that the relative standard deviations of counting rates are lower than 0.1%.

2.3.4. *HPGe gamma spectrometry*

Spectrometric measurements were carried out with an n-type HPGe detector calibrated with an efficiency curve obtained using a reference source traceable to international standards. Polyethylene vials prepared with aliquots from the five silicon solutions were measured for 70–125 h live-time to check for gamma-emitting impurities.

3. Results

3.1. *Gamma spectrometry*

No gamma-emitting impurity was observed within the detection limits in the HPGe-spectra acquired for all the samples prepared from the M32Si1-5 solutions.

3.2. *TDCR and CNET standardisations*

The efficiencies and activities were calculated with our own Fortran

code which takes the PMTs asymmetry and the micelle effect into account (Nedjadi et al., 2017). The code combines the detection efficiencies of ^{32}Si and its ^{32}P progeny using

$$\varepsilon_n = \varepsilon_{n,Si} + \alpha \bullet \varepsilon_{n,P} \qquad (1)$$

where the index n = AB, BC, AC, D, T refers to any of the various double coincidences between the three PMTs, denoted as A, B and C, the logical sum of double coincidences (D) or the triple coincidence (T). The coefficient α is the equilibrium factor computed at the mid-measurement time using a half-life of 14.284(36) for ^{32}P and 157(7) years for ^{32}Si (Bé et al., 2011 and 2013; NNDC, 2020). CNET double detection efficiencies were also computed using (1) and assuming PMT symmetry.

The code computes the detection efficiencies separately for each nuclide before combining them. It uses routines that calculate the beta spectrum functions of ^{32}Si and ^{32}P at any energy point. Maximum beta energies of 227.2(3) keV (Ouellet and Singh, 2011) and 1710.66(21) keV (Bé et al., 2011, 2013) are assumed for ^{32}Si and ^{32}P, respectively. The spectra functions include the screening, finite size, recoil and radiative corrections. The atomic exchange correction factors were provided by Mougeot (Mougeot, 2021).

The code calculates the ionisation quenching function by integrating the Birks' function with the ESTAR stopping powers of Berger, which include collisional and radiation stopping powers (Berger, 1993), or those of Gümüş (Gümüş et al., 2010) or Tan and Xia (2012), or by using Grau Malonda's parametrisation (Grau Malonda et al., 1999).

3.2.1. Activity determination of the M32Si1 solution

Fig. 2 compiles the TDCR and CNET activities obtained for M32Si1. The TDCR activities displayed are the means of 7, 20 and 9 counting points in the case of defocusing, grey filtering or quenching, in that order. The uncertainty bars shown are just the standard deviations of the counting points of the measurement. ESTAR stopping powers and an ionization quenching factor (kB) value of 0.075 mm MeV^{-1} were used throughout. A value of 0.12 mm MeV^{-1} yields activities that are, on average, 0.2% higher; this kB dependence is considered in the uncertainty budget. Including the atomic exchange correction in the beta spectrum increases the activity concentration by 0.2%.

The values obtained by defocusing are close to each other but are larger than those predicted by the grey filtering and chemical quenching measurements. The quenching measurement is 0.3% higher than the

grey filtering one, and 0.6% smaller than the average of the defocusing measurements. These differences are rather unusual. Furthermore, the average TDCR value is 0.9% higher than the CNET prediction; this deviation between the methods is larger than expected.

The figure also shows that measurements with HDPE vials yield somewhat higher activities than measurements with glass vials, which prompted us to monitor the stability of samples over time. The TDCR measurements were repeated for all samples eight months later. All samples were vortex-shaken, centrifuged, and left 24 h in the dark prior to re-measuring them. For HDPE vials, the activity decreased by 0.6% in the case of defocusing measurements and by only 0.1% for grey filtering and quenching. With regard to glass vials, the activity of the defocusing measurements dipped by 2.8% and that of the filtering measurement by 3.3%. The corresponding drop of the TDCR value was only about 0.7% in both cases, suggesting that radioactive silicon adsorbs into the walls of the vials over time. The use of glass vials was henceforth excluded for standardising this radionuclide.

The sample stability when using HDPE vials was monitored with weekly CNET measurements over a period of two months. Both the silicon vials and the tritium quenched sources were measured weekly. Results are shown in Fig. 3. The activity decrease is about 0.7% over one month. Notice however that there is a full recovery of the activity, even after eight months, if the vials are shaken prior to repeat measurements, suggesting that the drop in the activity of these vials may stem from a deterioration of the emulsion, i.e. a gradual breakup of micelles and a build-up of HSiA matter at the walls of the vials.

However, these medium-term instabilities cannot explain the rather unusual differences observed in Fig. 2, since the TDCR and CNET measurements shown there were made within three days.

A plausible explanation for these discrepancies may be the presence of tritium in the solution, as proposed by Kossert (Kossert et al., 2023). Using a liquid scintillation spectrometer with a logarithmic amplifier, which we do not have access to in our laboratory, the PTB inferred the presence of tritium with an activity ratio of about 3.14% on 1 May 2020. To reanalyse our TDCR and CNET measurements with this hypothesis, we rewrite the double and triple detection efficiencies in the following way:

$$\varepsilon_n = \varepsilon_{n,Si} + \alpha_{P-Si} \bullet \varepsilon_{n,P} + \theta \bullet f(\lambda_{Si}, \lambda_H) \bullet \varepsilon_{n,H} \qquad (2)$$

where the index n = AB, BC, AC, D, T to refer to any of the various
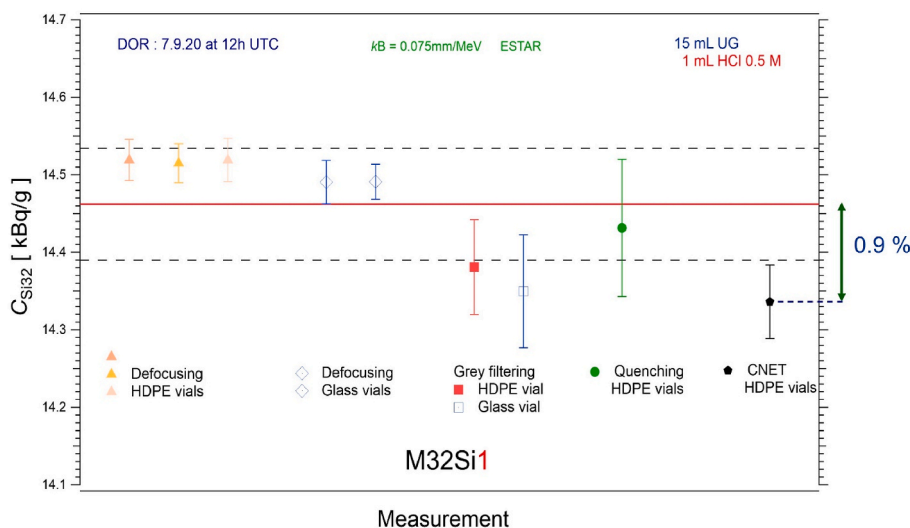

Fig. 2. TDCR and CNET activity measurements of M32Si1. All measurements refer to one source except for the quenching measurement which involves nine sources and the CNET value which is the average of three sources. The CNET measurement is indicated as a pentagon. The rest are TDCR determinations, the relevant efficiency variation method being indicated in the legend. The red line is the arithmetic average of all TDCR measurements. Standard uncertainties ($k=1$) are given in all cases. The TDCR uncertainty bars include only the standard deviations of the activities entailed by the counting points constitutive of a single measurement. The dashed lines indicate the full TDCR standard uncertainty estimated using the same procedure described in section 3.2.2.
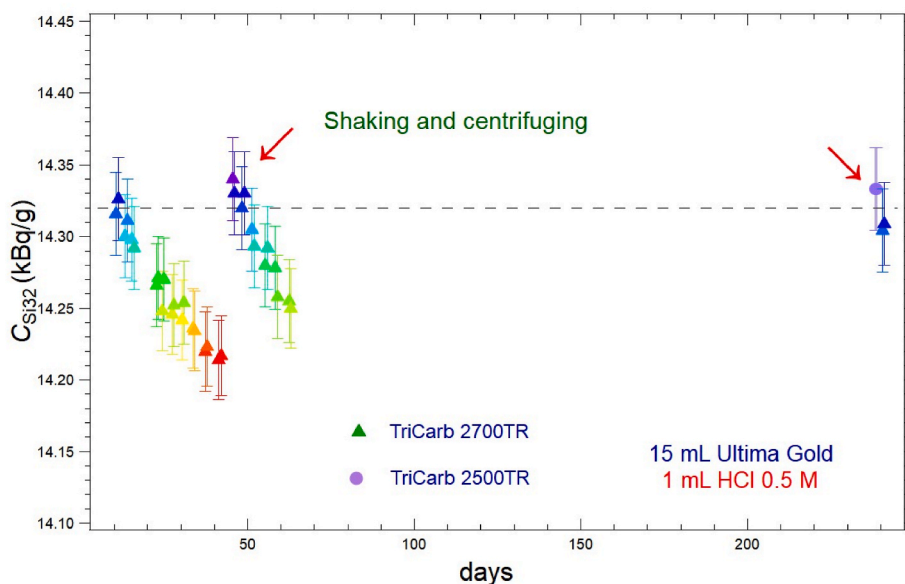
Fig. 3. Variations in activity concentration of M32Si1 in HDPE vials over time. Triangles denote measurements on the TriCarb 2700 TR while the circle refers to measurement on the TriCarb 2500 TR. The arrows indicate times at which the vials were shaken with a vortex shaker, centrifuged and stored in the dark one day before use.

double coincidences between the three PMTs, denoted as A, B and C, the logical sum of double coincidences (D) or the triple coincidence (T). The indices Si, P and H refer to ^{32}Si, ^{32}P and ^{3}H respectively. The coefficient $\alpha_{P\text{-}Si}$ is the equilibrium factor, θ is the ^{3}H–^{32}Si activity ratio, while f $(\lambda_{Si}, \lambda_H)$ denotes the time-dependent ^{3}H–^{32}Si decay factor ratio.

Assuming the presence of a tritium impurity does improve the consistency of the TDCR and CNET measurements, as displayed in Fig. 4. The quenching and grey filtering measurements agree within less than 0.1%, and both agree with the defocusing determination within 0.3%. The TDCR average and the CNET value are now 0.56% apart but remain compatible within one standard uncertainty. To avoid repetitions, the full TDCR and CNET uncertainty budgets are explained in detail in the next section.

3.2.2. Activity determination of the M32Si2 solution

Surmising the M32Si1 solution may contain tritium traces despite undergoing five evaporations to complete dryness, the M32Si2 solution

was desiccated ten times.

Fig. 5 outlines the activity concentrations predicted by the TDCR and CNET measurements. ESTAR stopping powers and a kB value of 0.075 mm MeV^{-1} are used throughout. The TDCR activities shown are the average of 7, 17 and 11 counting points in the case of defocusing, grey filtering or quenching, respectively. The defocusing activities match within 0.08%, and their average is consistent with the grey filtering and quenching values within 0.03% and 0.08% – in that order. Combining the TDCR activity concentrations gives an arithmetic mean of 109.52 kBq g^{-1} at the date of reference, shown as a red line. It differs by only 0.02% from the CNET determination, which is the average of five samples measured four times within a week. If the odd inconsistencies found in the M32Si1 standardisation pointed to the presence of an impurity, the coherence of these measurements may be indicative of the opposite conclusion.

The full uncertainty budget is detailed in Table 1. For the counting statistics contribution, one thousand sets of correlated random Gaussian
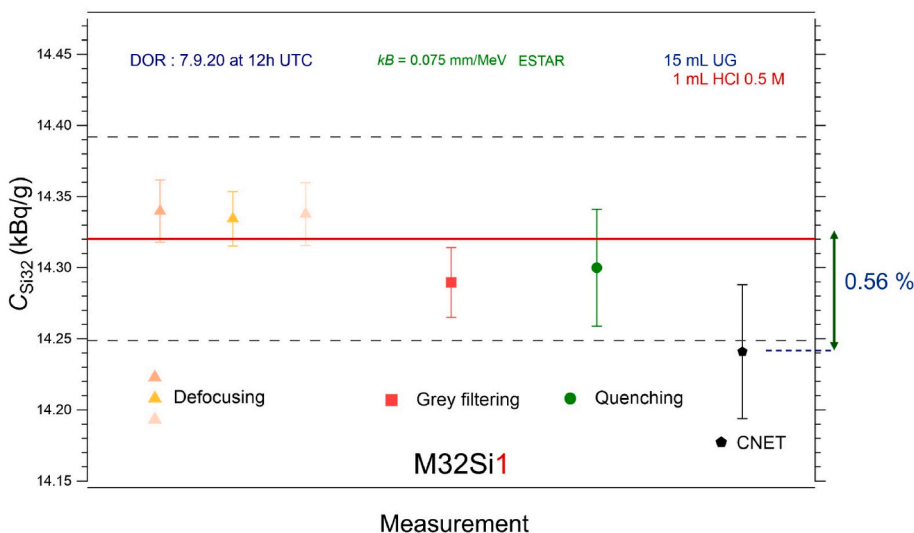

Fig. 4. ^{32}Si activity values for the M32Si1 solution when assuming the presence of tritium. The same legend as in Fig. 2 is used. Only HDPE vials are shown. The red line is the arithmetic average of all TDCR measurements.
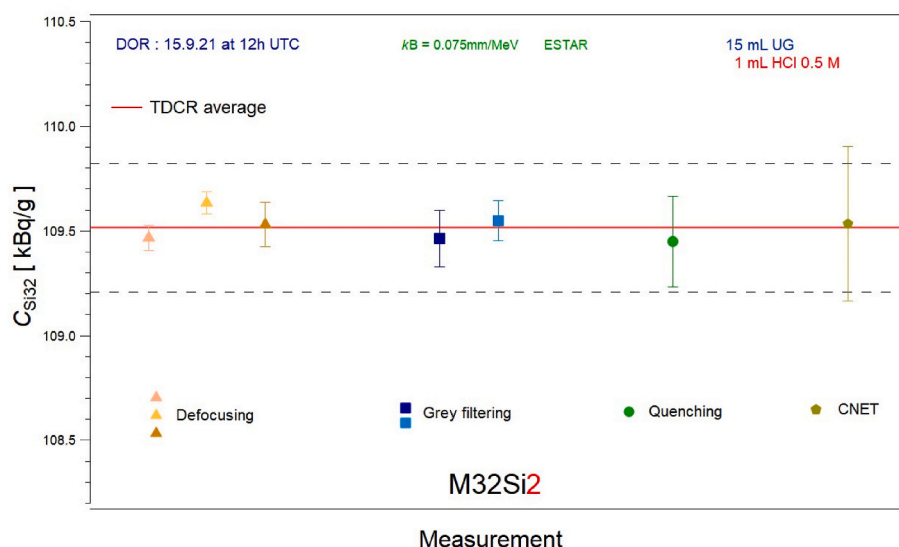
Fig. 5. TDCR and CNET activity measurements of the M32Si2 solution. Only HDPE vials are used. Standard uncertainties ($k=1$) are shown throughout. The TDCR uncertainty bars include only the standard deviations of the activities entailed by the counting points constitutive of a single measurement. The dashed lines indicate the full TDCR standard uncertainty (see section 3.2.2 and Table 2).

Table 1
Liquid scintillation counting uncertainty budgets for M32Si2. Uncertainties are given with $k = 1$.

Uncertainty item	Value in %	
	TDCR	CNET
Counting statistics	0.12	0.10
Background	0.01	0.01
kB & Q(E)	0.20	0.20
Tracer activity & tSIE		0.10
Decay correction	0.03	0.03
Dead-time	0.05	0.09
Weighing	0.11	0.11
Reproducibility/Repeatability	0.10	0.20
Combined uncertainty	0.29	0.35

net coincidence counting rates were generated for each of the counting points of a defocusing measurement. These sets of Monte Carlo simulated rates were built in such a way as to reproduce the experimental moments and covariance matrices. These rates are then read by the code that computes the efficiencies and activities. The ESTAR stopping powers are used and the *kB* parameter was fixed at 0.075 mm/MeV. The standard deviation of the distribution of the activities thus computed is taken to be the propagation of the rates' probability density functions on the activity.

The background component was estimated in a similar way using a defocusing measurement. One thousand sets of correlated random Gaussian background coincidence counting rates were generated for each counting point. The randomly generated rates have mean values, standard deviations of the means and covariance matrices which match those of the measured background rates. Corresponding net counting rates are calculated by subtracting the Monte Carlo background rates from the measured gross counting rates. Efficiencies and activities are then computed for these 10^3 defocusing data sets. The standard deviation of the distribution of the activities found in this way is the propagation of the background uncertainty on the activity.

Since the *kB* parameter and the electron stopping powers are correlated through the Birks formula, it is not possible to propagate their uncertainties independently. Therefore, separate sets of 2×10^3 uniform deviations of kB between 0.075 and 0.120 mm/MeV were generated at random, using a rectangular distribution, and then adjoined to five ionisation quench functions (discussed in section 3.2) to calculate a sum of 10^4 activities. This calculation was carried out for a defocusing measurement. The relative standard deviation of the 10^4 activities obtained with this procedure is 0.2%.

The uncertainty contribution assigned to the decay correction was estimated conservatively, assuming 50 years rather than 7 years for the half-life uncertainty, as the propagation of the half-life uncertainty to the decay correction factors. The reproducibility component was estimated as the relative standard deviation of six activities obtained with the three efficiency variation methods. The TDCR combined relative standard uncertainty obtained from the quadratic sum of these contributions is 0.29%.

For the CNET determination, the main contributions are from the uncertainty on the *kB* value and the stopping power model, which were propagated on the activities as detailed above, and the repeatability, i.e. the relative standard deviation of the four measurements of five sources within a week. The CNET combined relative standard uncertainty is 0.35%.

3.2.3. Activity measurements of the M32Si3, 4 and 5 solutions

As part of a further probing of the presence of tritium, three solutions were prepared anew. The first, M32Si3, also underwent ten evaporations, whereas the M32Si4 and M32Si5 solutions were desiccated thirty and fifty times respectively.

Figures A–C in the supplementary material sum up the activity concentrations determined with the TDCR and CNET measurements for the solutions M32Si3-5 in that order, with the ionisation quenching function calculated with the ESTAR stopping powers and a *kB* value of 0.075 mm MeV [1]. The TDCR values displayed are the means of 7 counting points in the case of defocusing, 18 in the case of grey filtering and 11 for quenching. The coherence of the activity determinations is robust for the three solutions. The activities obtained through defocusing agree within 0.15% for M32Si3 and within less than 0.03% for the other two solutions. The mean value of the defocusing measurements is consistent with the grey filtering and quenching measurements within less than 0.1% in all cases.

Combining the TDCR activity measurements gives a value of 17.54 (5) kBq g^{-1} for M32Si3, 26.91(7) kBq g^{-1} for solution M32Si4, and 36.20(10) kBq g^{-1} for M32Si5, at the same date of reference indicated in the figures. Uncertainties were estimated as explained in 3.2.2. The

relative differences between the TDCR and CNET determinations are 0.08%, 0.02%, and 0.03% for M32Si3-5 in that order.

No significant difference exists between the activity standardisations of these three solutions, suggesting the redundance of ever more desiccations to remove hypothetical tritium traces, which supports the view that tritium is absent or below detection levels in these solutions.

3.2.4. Activity standardisation of the M32Si6 solution

Concerned that no stability monitoring was performed on the samples prepared from the M32Si2 solution, and that activity differences between our laboratory and the PTB for this solution might be due to sample matrices, an additional 1.5 g aliquot, from the stock solution from which M32Si2 derives, was requested from the PSI. As the stock solution has been stored in a plastic container that does not fully maintain the integrity of the activity concentration of its content, this new aliquot is denoted M32Si6. As indicated in section 2.2.1, this solution was used to prepare the normal samples with UG cocktail and HCl 0.5 mol/L top-ups (6.5% aqueous fraction), in addition to samples with no top-up or with a water top-up matching in volume the deposited silicon drop.

The activity concentrations found with the TDCR and CNET methods are presented in Fig. 6. The same approach as above is used for the ionisation quenching function. Defocusing, grey filtering or quenching values are the means of 7, 17 and 11 counting point determinations respectively.

For vials with 1 mL hydrochloric acid top-up (filled markers) the situation is not much different from that shown in Fig. 5, for M32Si2. The defocusing, grey filtering and quenching determinations are consistent to within 0.1%. Combining the TDCR values for this type of sample yields a mean activity of 109.94 kBq g^{-1}, displayed as a red line, which differs by 0.14% from the CNET average of five such samples measured four times within a week. Note that this average M32Si6 TDCR activity is greater (0.31%) than that of the M32Si2 solution, probably reflecting the mass loss of the stock solution during storage.

Samples prepared with additional water (with an aqueous fraction of 0.2% or with no aqueous top-up), shown with empty markers, present a visible anomalous or inconsistent pattern. Samples with only a radioactive deposit fare the worst: 1% deviation for defocusing measurements

and 0.8% in the case of grey filtering.

This prompted a stability monitoring of these three types of samples (one of each) by defocusing TDCR measurements once every 3 weeks for about 2 months. Results are shown in Fig. 7. Samples with hydrochloric acid top-up are stable and yield a larger activity than the other two matrix choices which display marked time variations. Samples with water or no top-up have activities on average 0.25% and 1.0% lower than the one with additional hydrochloric acid.

This observation is corroborated by the monitoring with CNET measurements over a period of eight months of four samples with HCl top-up, presented in Fig. 8. In contrast to the striking drop in activity found for the M32Si1 solution (see Fig. 3), the M32Si6 (and hence M32Si2) solution exhibits a stable trend over time. This difference in stability may be in part due to the concentration of non-radioactive silicon which is much higher in M32Si6/2 than in M32Si1, a result of the larger number of processed vanadium disks in the former compared to the latter. In fact, the amount of processed vanadium disks is directly linked to the final silicon concentration in the final eluate. The concentration of stable silicon (sum of ^{28}Si, ^{29}Si, and ^{30}Si) in M32Si6/2 is around 20 μg/g (about 400 μg in total, considering seven vanadium disks), whereas its concentration in M32Si1 is only about 3 μg/g solution, as only one proton-irradiated vanadium disk was utilised to prepare this solution.

3.3. Coincidence efficiency tracing with ^{60}Co

3.3.1. 4πβ(LS)-γ(NaI) coincidence tracing of the M32Si1/6 solutions

Before proceeding with the measurements, verification was made that the ^{32}Si, ^{32}P and ^{60}Co beta efficiencies are related in such a way that increasing experimentally the ^{60}Co efficiency would also increase those of ^{32}Si and ^{32}P. Using the theoretical beta spectra of these nuclides, a simple model assuming increasing low-energy discrimination gives the relationships between the relative inefficiencies of these nuclides shown in Fig. 9. Within the range of ^{60}Co efficiency variation planned, a quasilinear relationship exists between the beta inefficiencies of these nuclides, thus justifying the efficiency extrapolation for the mixed sources.

A typical measured β-spectrum of a ^{32}Si–^{60}Co mixture is shown in Fig. 10. Typically, the β-channel detection efficiency (ε_β) was decreased
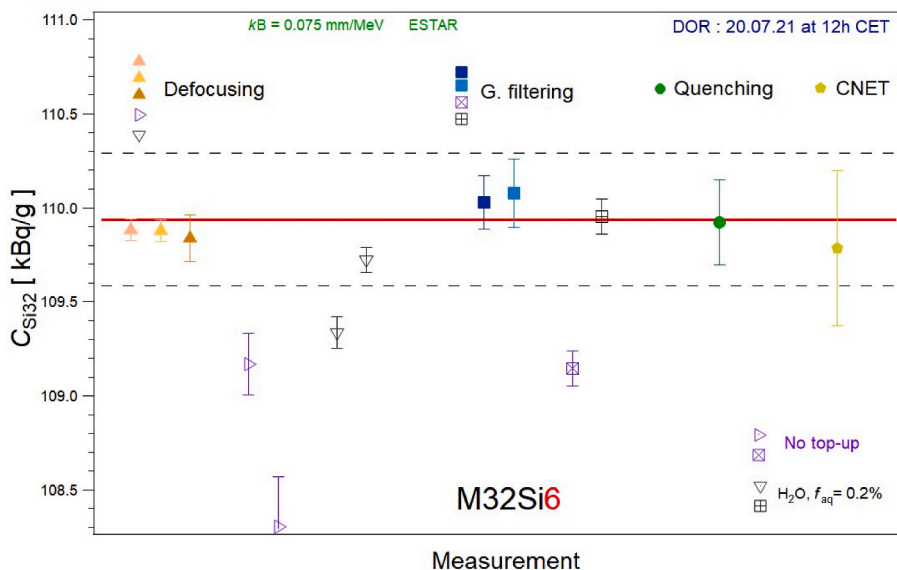

Fig. 6. Results of TDCR and CNET activity measurements of M32Si6. The red line is the arithmetic average of all TDCR measurements of samples with HCl 0.5 M top-up (f_{aq} = 6.5%). The filled markers concern such samples, while empty markers refer to samples with no top-up or water top-up as indicated in the bottom right. The types of efficiency variation are indicated in the legend. The TDCR uncertainty bars include only the standard deviations of the activities entailed by the counting points of the measurement. The CNET value is shown as a pentagon. The rest are TDCR determinations, the relevant efficiency variation method being indicated in the legend. Standard uncertainties (*k=1*) are given in all cases.
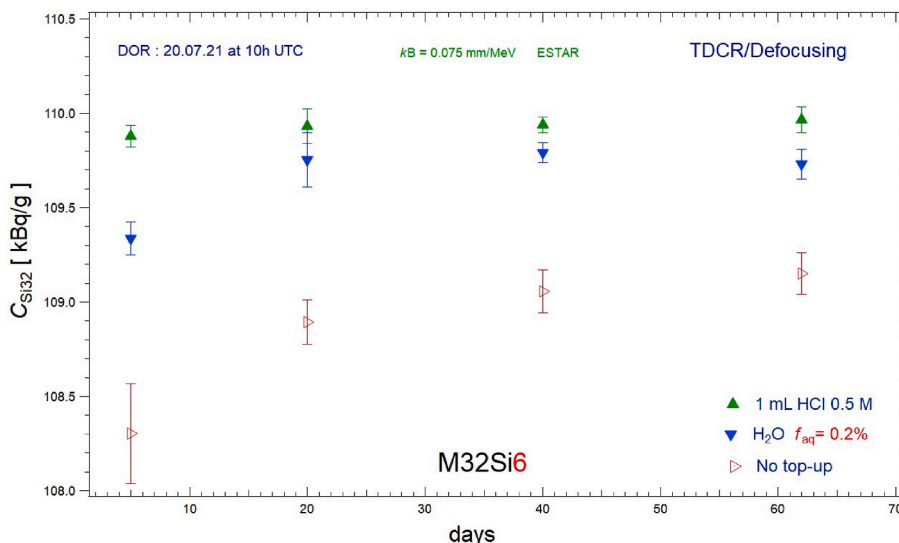
Fig. 7. Variation over time of the TDCR activity concentration of three samples with different matrices. Green triangle-up refer to the sample with 1 mL HCl 0.5 M top-up, the blue down triangles stand for the sample with a water addition that corresponds to the volume of the radioactive deposit, whereas the red right-triangle denotes the sample with no addition.
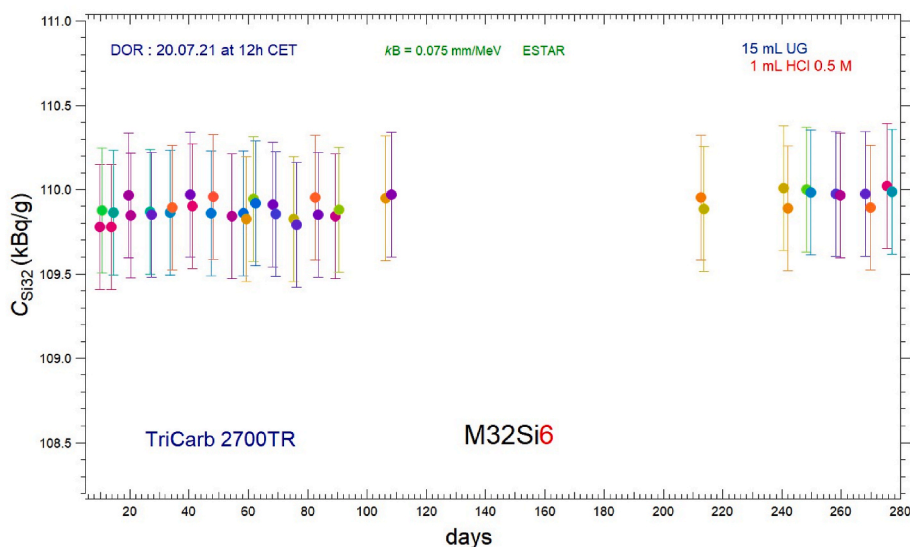

Fig. 8. Variation over eight months of the CNET activity concentration of four samples with 1 mL HCl 0.5 M top-up. Each marker is the average activity of the four samples. Measurements were carried out on a TriCarb2700. A set of quenched tritium standards was repeatedly measured in tandem with the silicon samples.

from a maximum of 92% down to around 55%. Countrates in this channel varied from 15 to 10 kcps for the source with the lowest silicone-cobalt activity ratio, and from 47 to 31 kcps for the source with the largest silicone-cobalt activity ratio.

The measurements were carried out with two gamma channel settings: a discrimination threshold at 43 keV, and a second one at 661.7 keV. The γ-detection efficiencies for these two settings were around 8.2% and 3.9%, respectively, at these two thresholds, for the source with the smallest ^{32}Si–^{60}Co activity ratio, and around 3.0% and 1.4%, respectively, for the source with the largest ^{32}Si–^{60}Co activity ratio.

Fig. 11 displays the efficiency extrapolations at these two gamma energy regimes for a ^{60}Co source prepared from the solution used to prepare mixed silicone-cobalt sources. The corresponding efficiency extrapolations for one of the ^{32}Si–^{60}Co sources are shown in Fig. 12. In both figures, linear fits are adequate for modelling the data throughout the efficiency coverage, and the data at the two gamma conditions

converge well. The same holds for the other two mixed sources, but for the source with the highest ^{32}Si–^{60}Co activity ratio, the experimental data are better described with a quadratic efficiency function. This is probably a result of the inadequacy of the pulse shaping we used for this very high counting rate source rather than some self-absorption inside it. The presence of tritium residues in the silicon solution could also contribute to the non-linearity (see below in section 4).

The residuals of the linear efficiency extrapolation least-square fit, for the two gamma settings in the case of a mixed silicone-cobalt source, are displayed in Fig. 13 as an example. The residuals are presented just to illustrate the scatter of the data. In practice, these simple fits are not used to determine the activity concentration. Instead, Monte Carlo linear fits that take the uncertainties of both ε_β and $\rho_\beta\rho_\gamma/\rho_c$ into account (Nedjadi et al., 2012) are performed. Ten thousand fits are made by varying stochastically $(1-\varepsilon_\beta)/\varepsilon_\beta$ and $\rho_\beta\rho_\gamma/\rho_c$ within their distributions assumed to be Gaussian. The mean of the intercept distribution is then
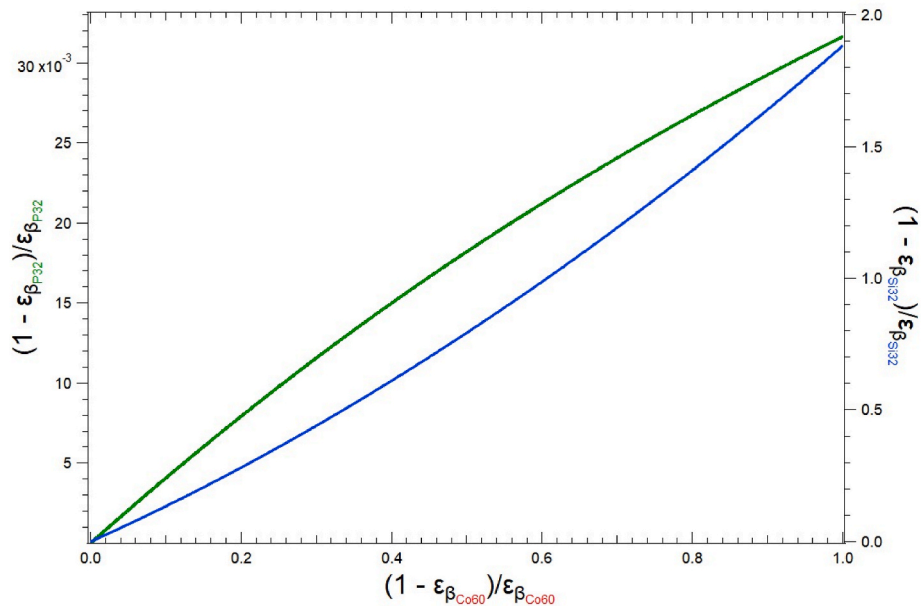
Fig. 9. Relationship between the ^{32}Si and ^{32}P relative inefficiencies against that of ^{60}Co using theoretical spectra and low-energy discrimination.

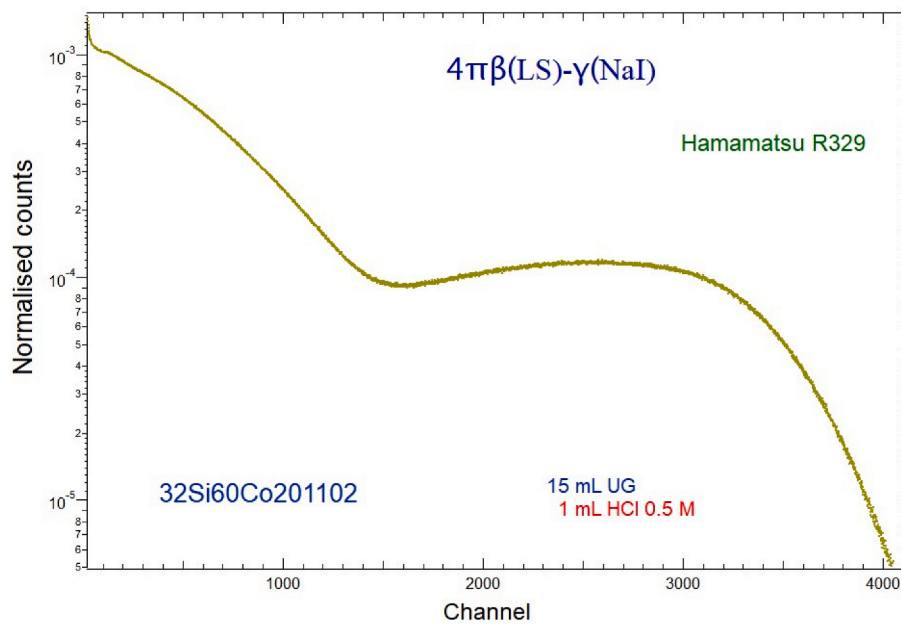**Fig. 10.** ^{32}Si–^{60}Co beta spectrum obtained with Ultima Gold scintillator and a 2-inch photomultiplier tube.

considered to be the actual intercept while the standard deviation of the distribution is estimated to be the intercept uncertainty.

Table 2 lays out the intercepts found for a cobalt source and the four mixed ^{32}Si–^{60}Co sources in the two gamma settings. The Si–Co activity ratio is indicated for each mixed source. The degrees of freedom of the linear efficiency extrapolations range from 30 to 40, with an average of 35. The uncertainties shown are the standard deviations of the intercept distributions, as described above. The intercepts for the 661.7 keV threshold have bigger uncertainties, because of the lower gamma detection efficiency. The intercepts for the two gamma settings are consistent within 0.2% for the three sources with an ^{32}Si–^{60}Co activity ratio lower than 2, and within 0.7% for the very active source. The arithmetic mean activities of the three mixed sources agree within 0.1%. The last column on the right lists these mean activities with their full

uncertainties. Combining the activity concentrations of the three sources, obtained with *linear* efficiency extrapolations, gives an arithmetic mean of 14.395(84) kBq g^{-1} at the date of reference.

Table 3 spells out the uncertainty budget adopted for these coincidence measurements with efficiency tracing. The uncertainty of the tracer activity (^{60}Co) dominates the uncertainties. A median value of the relative standard deviations of the intercept distributions of all the measurements was used as the Monte Carlo extrapolation uncertainty. The counting statistics stands for a typical standard deviation of the mean of $\rho_\beta \bullet \rho_\gamma / \rho_c$. Reproducibility is the relative standard deviation of six efficiency-extrapolated activities obtained with three sources and two gamma settings. The combined uncertainty obtained from the quadratic sum of the uncertainty components is 0.59% ($k=1$).

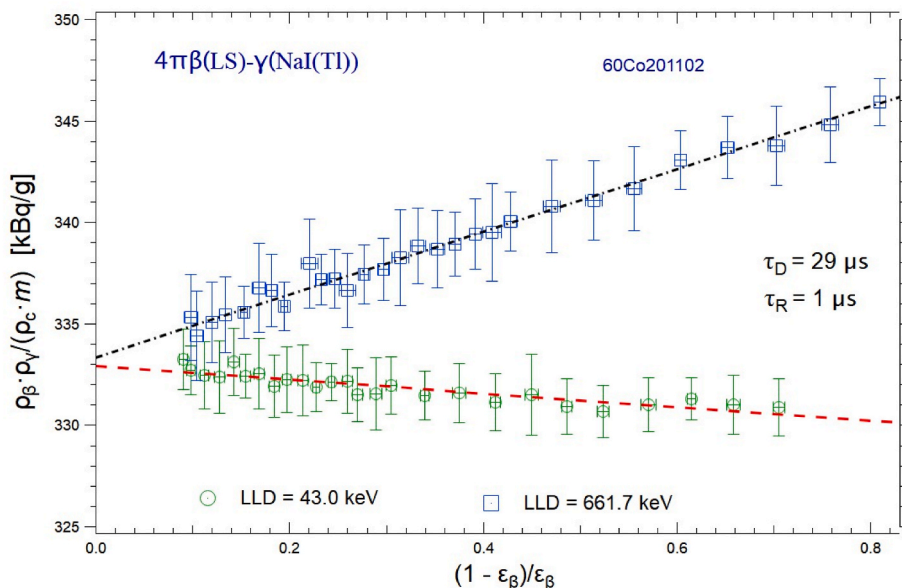Finally, the M32Si6 solution was also standardised using the same

Fig. 11. ^{60}Co 4πβ(LS)-γ(NaI) efficiency extrapolation curves. Green circles stand for a threshold at 43.0 keV while blue squares represent a threshold at 661.7 keV. The lines are linear fits.
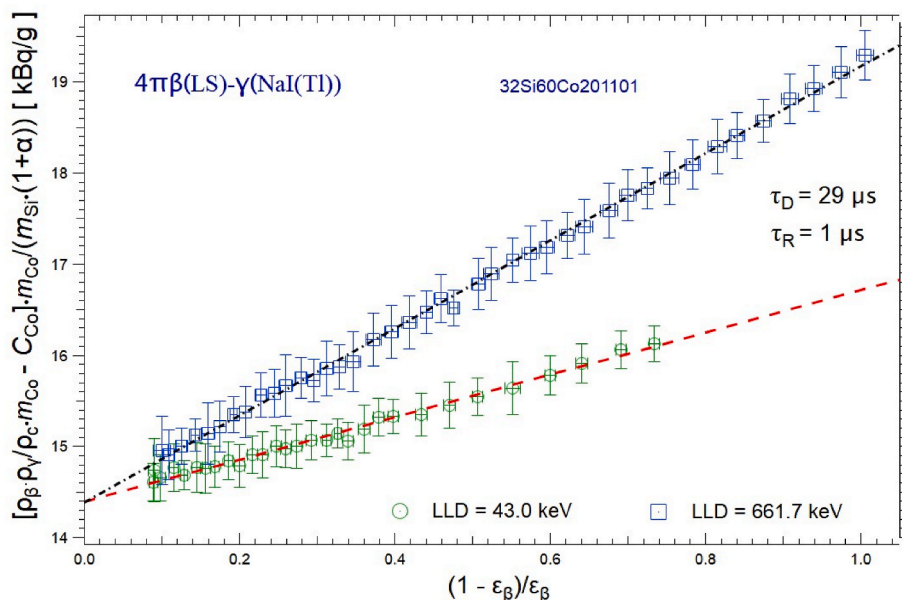

Fig. 12. ^{32}Si–^{60}Co 4πβ(LS)-γ(NaI) efficiency extrapolation curves for the M32Si1 solution. Green circles show measurements at a 43.0 keV γ-threshold, while the blue squares depict values obtained for a threshold at 661.7 keV. The lines are linear fits.

technique but with using a fast digitizer to obtain data in list-mode format in addition to a custom-built software for a subsequent offline-analysis. In this case, the activity concentration found was 110.25(44) kBq/g.

3.3.2. 4πβ(PS)-4πγ(NaI) coincidence tracing of the M32Si2 solution

The β-spectra obtained for mixed ^{32}Si–^{60}Co sources using UPS923A plastic scintillators and a one-inch PMT have a typical shape presented in figure E in the supplementary material. However, unlike the high beta detection efficiencies obtained in the 4πβ(LS) case, here they are drastically reduced because of the crystal structure, shown in Fig. 1, which causes a strong self-absorption. The maximum ε_β obtained for these sources was 50.3%. Using the Ludox seeding agent to homogenise the crystallisation during the drying process did not mitigate much the beta

efficiency loss. ε_β was varied by electronic discrimination to a minimum of 20.0%. Beta counting rates ranged from 9.2 to 15 kcps for the most active ^{32}Si–^{60}Co source, and between 4.0 and 7.4 kcps for the least active one. The background rate was in the 0.3–1.2 cps range.

A typical 4π gamma-ray spectrum of the mixed sources is presented in figure F in the supplementary material. Here, a discrimination threshold at 59.5 keV and another one at 661.7 keV were used. For the source with the minimum ^{32}Si–^{60}Co activity ratio, the γ-detection efficiencies were respectively 55% and 43% at these two thresholds. For the one with the maximum activity ratio, they were 31.0% and 27.7%, respectively.

Fig. 14 reports the efficiency extrapolations for a ^{60}Co plastic scintillation tracer source at the two gamma-thresholds (59.5 keV and 661.7 keV). High beta efficiencies are achieved, and the linear fits are adequate
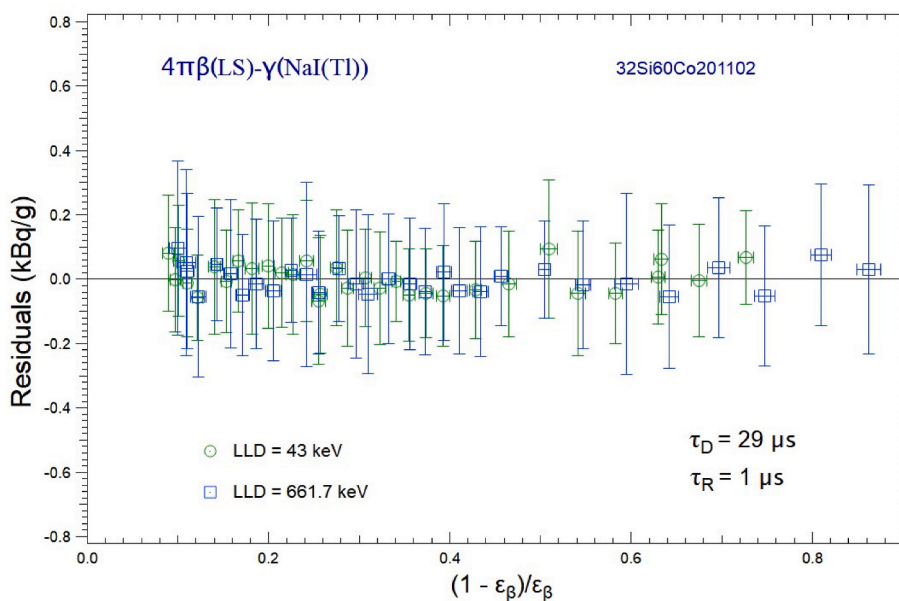
Fig. 13. Residuals of the 4πβ(LS)-γ(NaI) efficiency extrapolation for the M32Si1 solution.

Table 2
Extrapolated activity concentrations of M32Si1. The reference date is 7.9.2020 at 12h UTC. Uncertainties are given with $k = 1$.

Source	$A_{Si}/$ A_{Co}	Activity concentration in kBq/g		
		43.0 keV γ-threshold	661.7 keV γ-threshold	Average
60Co201102		332.91 ± 0.45	333.41 ± 0.58	333.16 ± 0.82
32Si60Co201101	0.26	14.399 ± 0.071	14.376 ± 0.095	14.388 ± 0.074
32Si60Co201102	0.43	14.401 ± 0.063	14.371 ± 0.079	14.386 ± 0.069
32Si60Co201103	0.93	14.390 ± 0.058	14.372 ± 0.072	14.381 ± 0.083
32Si60Co201104	2.02	14.653 ± 0.102	14.556 ± 0.136	14.605 ± 0.148

Table 3
Uncertainty budget for the ^{60}Co 4πβ(LS)-γ coincidence tracing of the M32Si1 solution.

Nature of uncertainty	Value in % ($k = 1$)
Background	0.063
Decay correction	0.002
Deadtime	0.041
Resolving time	0.005
Timing	0.002
Weighing	0.015
Tracer activity	0.246
Monte Carlo efficiency extrapolation	0.504
Counting statistics	0.100
Reproducibility	0.112
Combined uncertainty	0.59

for fitting the extrapolation functions.

The efficiency extrapolations for one of the ^{32}Si–^{60}Co sources are shown in Fig. 15. The efficiency functions begin at rather high relative inefficiencies and present a marked departure from linearity. This is quite different from the liquid scintillation coincidence situation where high efficiency and linear extrapolation ensue, as indicated in Fig. 12. The solid lines are quadratic fits throughout the efficiency range. The intercepts from such fits converge towards a value that is around 25%

higher than the expected activity concentration. This is clearly not satisfactory and is a consequence of the strong self-absorption inside the source caused by the crystal structure. Note that the mixed source prepared from a mixed ^{32}Si-^{60}Co solution, by contrast to topping a cobalt with a separate silicon aliquot, presented the same efficiency loss and non-linearity as exhibited in Fig. 15.

The dashed lines in this figure are linear fits of the portion of the data that behaves linearly, at much higher inefficiencies. These linear fits predict consistent intercepts that are close to the expected activity value, but they will not be used for the final results.

To demonstrate that the crystal structure is the actual cause of the severe efficiency loss, a ^{60}Co plastic scintillation source was prepared by adding Ludox and then an aliquot of lanthanum nitrate and ammonium hydroxide was drop deposited gravimetrically on top of the radioactive cobalt chloride. During the drying process a crystal structure, like the one shown in Fig. 1, formed. This ^{60}Co source was then measured in the 4πβ(PS)-4πγ(NaI) system. The resulting efficiency function, for a gamma threshold at 661.7 keV, is displayed in turquoise diamonds in Fig. 16. For contrast, the blue squares in the figure represent the same data for a normal ^{60}Co plastic scintillation source prepared with just the radioactive deposit from the same solution. Clearly the effect of adding lanthanum nitrate and ammonium hydroxide is to severely reduce the beta detection efficiency. There is however no breach of linearity suggesting that the non-linear behaviour of the efficiency functions displayed in Fig. 15 is attributable to the self-absorption of silicon in the crystal structure.

4. Discussion

Key findings of these exploratory measurements of the ^{32}Si test solutions prepared from proton irradiated vanadium disks pertain, first, to the stability of samples. No accurate activity standardisation of this nuclide can be performed with unsteady samples.

Three conditions are necessary for preparing stable samples with the hexafluorosilicic solutions. Firstly, HDPE vials should be used instead of glass ones as the latter adsorb radioactive silicon into their walls, probably through Si-ion exchange. When using samples in glass vials, the determined activity was found to be lower by about 3% after a period of 8 months. Secondly, samples should be topped-up with a large fraction of HCl 0.5 mol/L. Using water instead of HCl 0.5 mol/L top-up interferes with the speciation of the HSiA. Samples with only the
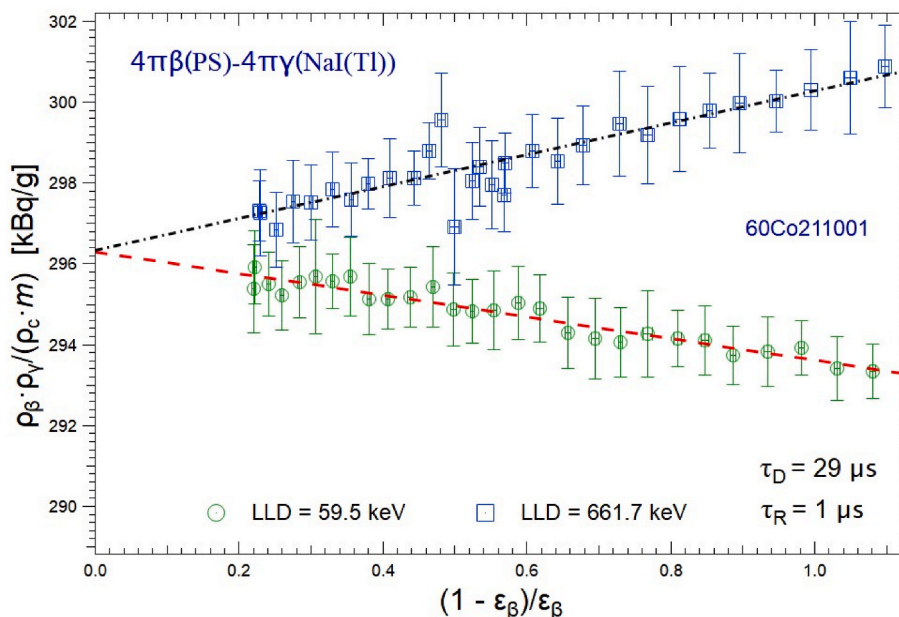
Fig. 14. $4\pi\beta(PS)$-$4\pi\gamma(NaI)$ efficiency extrapolation curves for the ^{60}Co tracer. Green circles are for a threshold at 59.5 keV whereas blue squares stand for a threshold at 661.7 keV. Linear fits are shown as dashed lines.
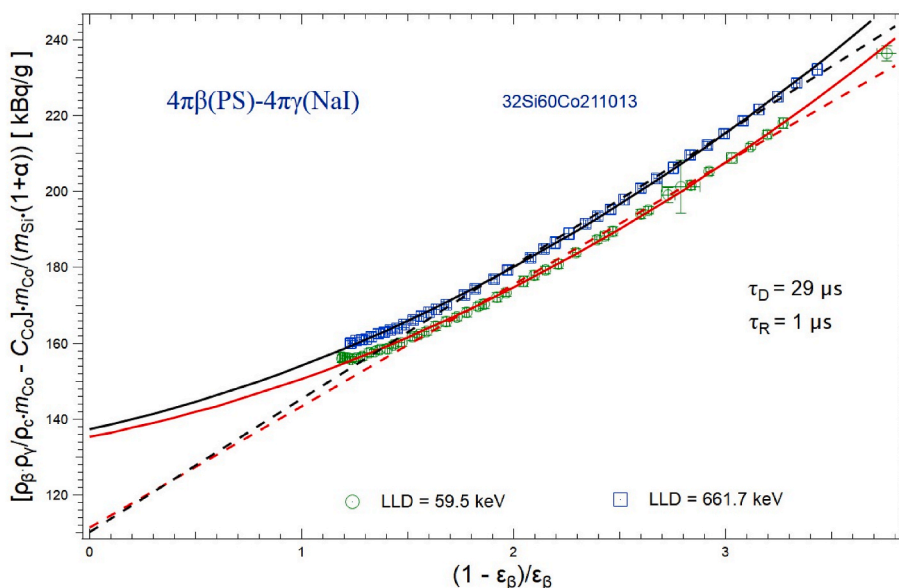

Fig. 15. ^{32}Si–^{60}Co $4\pi\beta(PS)$-$4\pi\gamma(NaI)$ efficiency extrapolation curves for the M32Si2 solution. Green circles and blue squares represent measurements at 59.5 keV and 661.7 keV γ-thresholds respectively. The solid lines show quadratic fits over the whole efficiency range, while linear fits of the high inefficiency range are displayed as dashed lines.

radioactive deposit or samples with small water top-ups were found to be unstable or to have up to 1% lower activities than samples to which about 1 mL of HCl 0.5 mol/L had been added after the HSiA aliquot. Thirdly, the radioactive silicon solution should have a sufficiently large concentration of non-active silicon. The contrast between the stability profiles of the M32Si1 and M32Si6 solutions, shown in Figs. 3 and 8 respectively, is stark. Non-active silicon mitigates the wall adsorption and the speciation issue.

Now regarding the activity standardisations, Table 4 summarises the values obtained for the various tested solutions using liquid scintillation counting and coincidence tracing with ^{60}Co.

For the M32Si1 solution, the TDCR measurements (defocusing, grey filtering, quenching) did not present their expected internal coherence

and were unusually higher (0.9%) than the CNET determination. Assuming this solution contained a tritium impurity quantified by the PTB improved the self-consistency of the TDCR measurements and reduced the discrepancy between the TDCR and CNET values to 0.56%.

This solution was also standardised with coincidence tracing with ^{60}Co. The tabulated arithmetic average of six efficiency extrapolations, obtained from three sources of varying silicon to cobalt activity ratio and two gamma thresholds, deviates by 0.03% from the liquid scintillation determination (arithmetic mean of TDCR and CNET activities) assuming no tritium impurity and by 0.79% if one assumes there is tritium at an activity ratio of 3.14% on 1 May 2020.

Concerned about the effect of the potential presence of tritium on the efficiency extrapolation in the coincidence tracing with ^{60}Co, four mixed
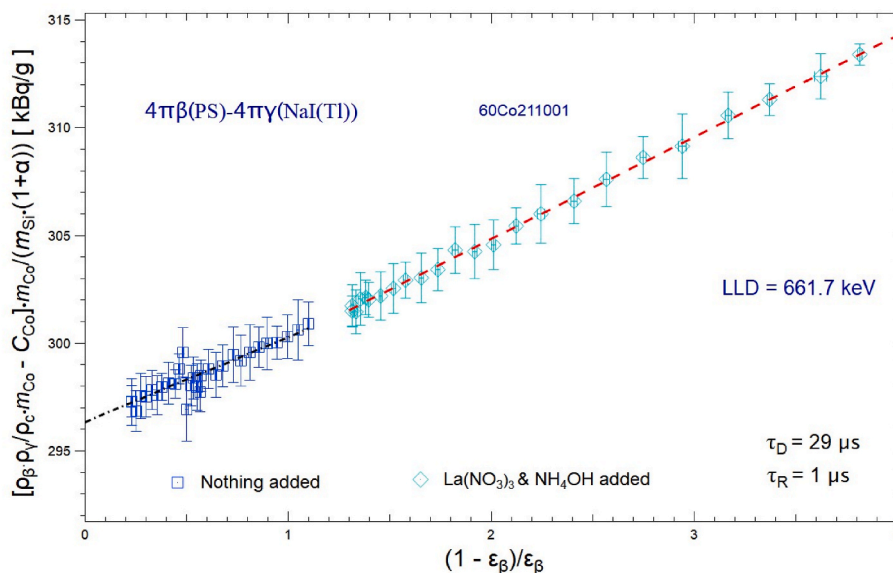
Fig. 16. Effect of the lanthanum nitrate and ammonium hydroxide on the ^{60}Co $4\pi\beta$(PS)-$4\pi\gamma$(NaI) efficiency extrapolation curve at the 661.7 keV threshold. Turquoise diamonds show data for a ^{60}Co plastic scintillation source prepared with a radioactive drop to which an aliquot of lanthanum nitrate and ammonium hydroxide was added immediately after deposition. Blue squares depict the same data for a normal ^{60}Co source prepared with only the radioactive deposit.

Table 4
Summary of the activity concentrations (kBq/g) of the various ^{32}Si solutions standardised. LS (Liquid Scintillation) indicates the average between the TDCR and CNET techniques. Uncertainties are given with $k = 1$.

Solution	TDCR	CNET	LS	$4\pi\beta$(LS)-γ	Reference date
M32Si1	14.46(7)	14.34(5)	14.40(7)	14.39(8)	07.09.2020 12h UTC
M32Si1[a]	14.32(7)	14.24(5)	14.28(7)		07.09.2020 12h UTC
M32Si2	109.52 (31)	109.53 (38)	109.53 (38)		15.09.2021 12h UTC
M32Si3	17.54(5)	17.55(5)	17.55(5)		01.11.2021 12h UTC
M32Si4	26.91(7)	26.92(9)	26.91(9)		01.11.2021 12h UTC
M32Si5	36.20 (10)	36.21 (12)	36.20 (12)		01.11.2021 12h UTC
M32Si6	109.86 (35)	109.77 (41)	109.86 (41)	110.25 (44)[b]	15.09.2021 12h UTC

[a] Assuming a tritium impurity and applying corresponding corrections.
[b] Acquisition was carried out with a fast digitizer.

^{3}H–^{60}Co liquid scintillation sources were prepared, with IRA-METAS tritiated water and ^{60}Co standards, in such a way as to vary the tritium-cobalt activity ratio (0.25%, 1%, 4.5% and 7.5%). These sources and a pure ^{60}Co source were measured with the system described in section 2.3.2 with a CeBr$_3$ detector for counting the gamma-rays. The effect of the presence of tritium on the efficiency function is shown in Fig. 17. The data in red shows the linear efficiency function for a pure ^{60}Co source. For the mixed source with 0.25% tritium-cobalt activity ratio, no effect is visible on the efficiency function, which is not shown so as not to clutter the figure. However, ^{3}H–^{60}Co mixed sources with higher activity ratios do introduce non-linearities in the efficiency profiles (blue, black and green).

A 3% tritium impurity activity ratio in the M32Si1 solution translates into 0.8%, 1.3%, 2.8% and 6.1% ^{3}H–^{60}Co activity ratios in the four ^{32}Si–^{60}Co mixed sources prepared for the coincidence tracing method. However, as discussed in 3.3.1, only the source with the highest ^{32}Si–^{60}Co activity ratio presented a quadratic rather than linear efficiency function. If there were a 3% tritium impurity activity ratio one would expect at least two of the ^{32}Si–^{60}Co mixed sources to present this

departure from linearity, which is not the case. This suggests that the 3% tritium activity ratio may be overestimated.

As regards the M32Si2 solution, which underwent ten rather than the five desiccations performed on M32Si1, the TDCR measurements display strong internal coherence (relative deviations lower than 0.1%) and their average matches the CNET mean value within 0.02%. Attempts to back up this activity determination with coincidence tracing with ^{60}Co using plastic scintillators failed because the addition of lanthanum nitrate and ammonium hydroxide to fix silicon onto the plastic during the drying process generated a thick energy-absorbing crystal structure which drastically cuts the beta detection efficiency and renders the efficiency function non-linear.

M32Si3-5 test solutions were evaporated 10, 30 and 50 times respectively to eliminate potential tritium residues. Their TDCR activity standardisations showed robust internal coherence, the defocusing, grey filtering and quenching measurements matching to within 0.1% (see figures A–C in the supplementary material). The averages of the TDCR determinations deviate by 0.08%, 0.02% and 0.03% from their respective CNET counterparts for the three solutions in that order. The activity measurements of these solutions did not reveal any compelling difference, thereby indicating that it is needless to desiccate more than ten times the HSiA to reduce hypothetical tritium traces below detection level.

Standardising the activity of the M32Si6 solution with the TDCR and CNET methods led to the same observations made for M32Si2, except that its activity values are 0.3% higher than those obtained for the latter, demonstrating that the plastic container, in which the stock solution has been stored, does not preserve the activity concentration of the solutions it holds. As shown in Table 4, the confirmatory standardising of this solution with ^{60}Co coincidence tracing corroborated the liquid scintillation counting average within 0.4%.

Comprehensive uncertainty budgets for the TDCR, CNET and coincidence tracing methods were given in Tables 1 and 3 and discussed in section 3. Even if these budgets are augmented to include uncertainties pertaining to activity concentration variations during storage, the full combined relative standard uncertainty ($k = 1$) of any of these techniques is unlikely to exceed 1%.
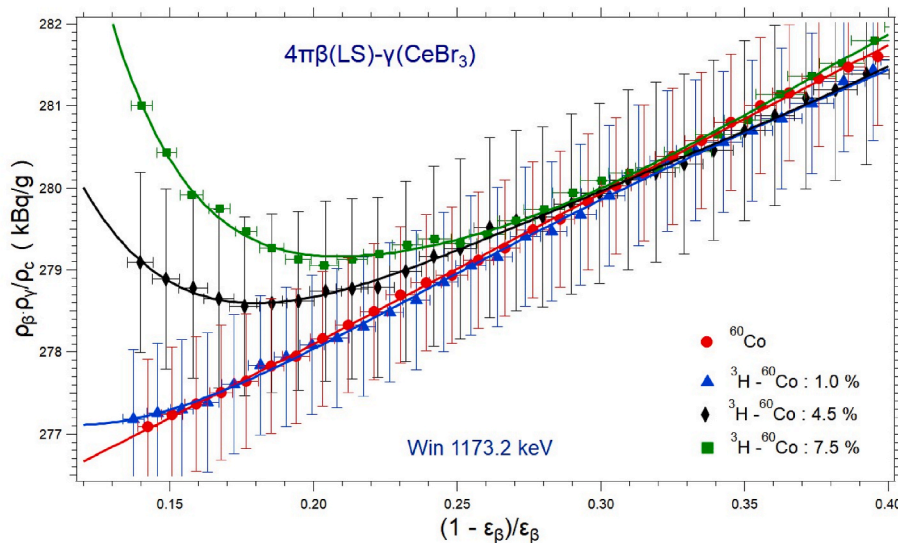
Fig. 17. Effect of tritium at different activity ratios on the ^{60}Co $4\pi\beta$(LS)-γ(CeBr$_3$) efficiency extrapolation curve for a window around the 1173.2 keV peak.

5. Conclusion

As part of the SINCHRON collaboration, which seeks to make a new precise determination of the ^{32}Si half-life with high activity sources, IRA-METAS standardised several test solutions over a period of three years.

These preparatory investigations identified the conditions necessary to make stable ^{32}Si liquid scintillation samples, i.e. the use of hexa-fluorosilicic acid solutions with a substantial non-active silicon content, preferring HDPE to glass vials, and topping-up the UG samples with large fractions of HCl 0.5 mol/L, representing the solution's matrix.

The TDCR measurements of the first test solution showed unexpected inconsistencies and their average unusually deviated by about 0.9% from the CNET measurement. Analysing samples from this solution with a Quantulus logarithmic amplification the PTB determined that a tritium impurity was present in the solution with an about 3% activity ratio. Allowing for this impurity improved the self-consistency of the TDCR measurements and reduced the TDCR-CNET discrepancy to about 0.6%.

The rest of the tested HSiA solutions underwent at least twice the desiccations performed on the first solution to eliminate tritium traces. The TDCR standardisations of these solutions using defocusing, grey filtering and quenching presented robust internal coherence in all cases, and the averages for these activity determinations closely matched the corresponding CNET measurements.

β-γ coincidence tracing with ^{60}Co was used as an independent method to probe the validity of these liquid scintillation measurements. It is to be noted that this method does not need a-priori knowledge about decay data such as beta spectrum shapes and maximum beta energies. The activity standardisation of the first solution with this technique, using a liquid scintillant for beta detection, predicted an activity concentration in agreement within a standard deviation with the liquid scintillation value, whether one considers the presence of tritium or ignores it. The effect of tritium on the efficiency extrapolation of ^{60}Co was investigated and shown to introduce a detectable non-linearity when the ^{3}H–^{60}Co activity ratio exceeds 1%. The analysis of the efficiency functions of the ^{32}Si–^{60}Co mixed sources suggests that the tritium content of the first solution may be overestimated. Finally, coincidence tracing with ^{60}Co was also used effectively to corroborate the liquid scintillation determination of the activity of the M32Si6 solution.

The attempt to implement this tracing technique with a plastic scintillator for beta detection was not successful. Adding lanthanum nitrate and ammonium hydroxide to prevent the volatility of silicon during the drying process created a chunky crystal structure. The self-absorption in the source severely reduced the beta detection efficiency and set non-linearities in the efficiency function.

The analyses of the uncertainty budgets of these techniques indicate that one can standardise the activity of the PSI hexafluorosilicic solutions with less than 1% relative standard uncertainty provided the stability conditions laid out above are met. This is an important step towards a new and precise half-life determination. However, such a determination also requires a precise determination of the number of ^{32}Si nuclei, which is not the subject of this article.

CRediT authorship contribution statement

Youcef Nedjadi: Writing – review & editing, Writing – original draft, Validation, Supervision, Software, Methodology, Investigation, Formal analysis, Conceptualization. **M. Teresa Durán:** Writing – original draft, Validation, Investigation. **Frédéric Juget:** Writing – original draft, Validation, Investigation. **François Bochud:** Resources, Project administration, Funding acquisition. **Mario Veicht:** Writing – original draft, Validation, Investigation, Formal analysis. **Dorothea Schumann:** Writing – original draft, Supervision, Resources, Project administration, Methodology, Investigation, Funding acquisition, Conceptualization. **Ionut Mihalcea:** Validation, Methodology, Investigation, Formal analysis. **Karsten Kossert:** Writing – original draft, Validation, Methodology, Investigation, Formal analysis, Conceptualization. **Claude Bailat:** Supervision, Resources, Project administration, Funding acquisition, Conceptualization.

Declaration of competing interest

The authors declare that they have no known competing financial interests or personal relationships that could have appeared to influence the work reported in this paper.

Data availability

Data will be made available on request.

Appendix A. Supplementary data

Supplementary data to this article can be found online at https://doi.org/10.1016/j.apradiso.2023.111041.

References

Aggarwal, P.K., Froehlich, K.F., Gat, J.R., 2007. Isotopes in the Water Cycle: Past, Present and Future of a Developing Science. Springer, Dordrecht, p. 197.

Baerg, A.P., Meghir, S., Bowes, G.C., 1964. Extension of the efficiency tracing method for the calibration of pure β-emitters. Int. J. Appl. Radiat. Isot. 15, 279–287.

Bé, M.-M., Chisté, V., Dulieu, C., Mougeot, X., Chechev, V., Kuzmenko, N., Kondev, F., Luca, A., Galán, M., Nichols, A.L., Arinc, A., Pearce, A., Huang, X., Wang, B., 2011. Table of Radionuclides: 22 to 242A', Monographie BIPM-5, 6. Bureau International des Poids et Mesures, Sèvres. ISBN-13978-92-822–2242-3.

Bé, M.-M., Chisté, V., Dulieu, C., Mougeot, X., Chechev, V., Kondev, F., Nichols, A.L., Huang, X., Wang, B., 2013. 'Table of Radionuclides: 14 to 245A', Monographie BIPM-5, 7. Bureau International des Poids et Mesures, Sèvres. ISBN-13978-92-822–2248-5.

Berger, M.J., 1993. ESTAR, PSTAR and ASTAR, a PC Package for Calculating Stopping Powers and Ranges of Electrons, Protons and Helium Ions. IAEA-NDS-144.

Bouchard, J., Chauvenet, B., 1999. A simple, powerful $4\pi\beta-\gamma$ coincidence system based on the pulse-mixing method. Nucl. Instrum. Methods 422, 395–399.

Bouchard, J., Cassette, P., 2000. MAC3: an electronic module for the processing of pulses delivered by a three photomultiplier liquid scintillation counting system. Appl. Radiat. Isot. 52, 669–672.

Broda, R., Cassette, P., Kossert, K., 2007. Radionuclide metrology using liquid scintillation counting. Metrologia 44, S36–S52.

Campion, P.J., Taylor, J.G.V., Merritt, J.S., 1960. The efficiency tracing technique for eliminating self-absorption errors in 4pb-counting. Int. J. Appl. Radiat. Isot. 8, 8.

Chun Guang Yan, C.G., Lian, Q., Li, W., Ni, J.Z., 2002. An improvement of uncertainty in activity standardization with efficiency tracer technique. Appl. Radiat. Isot. 56, 253–259.

Dutsov, C., Cassette, P., Sabot, B., Mitev, K., 2020. Evaluation of the accidental coincidence counting rates in TDCR counting. Nucl. Instrum. Methods A977, 164292.

Fifield, L.K., Morgenstern, U., 2009. Silicon-32 as a tool for dating the recent past. Quat. Geochronol. 4, 400–405.

Finney, W.F., Wilson, E., Callender, A., Morris, M.D., Beck, L.W., 2006. Reexamination of hexafluorosilicate hydrolysis by 19F NMR and pH measurement. Environ. Sci. Technol. 40, 2572–2577.

Grau Malonda, A., 1999. Free Parameter Models in Liquid Scintillation Counting. CIEMAT, Madrid.

Grau Malonda, A., Grau Carles, A., 1999. The ionization quench factor in liquid-scintillation counting standardizations. Appl. Radiat. Isot. 51, 183–188.

Gümüş, H., Kabadayi, Ö., 2010. Practical calculations of stopping powers for intermediate energy electrons in some elemental solids. Vacuum 85, 245–252 and private communication.

Lal, D., Nijampurkar, V.N., Somayajulu, B.L.K., Koide, M., Goldberg, E.D., 1976. Silicon-32 specific activities in coastal waters of the world oceans. Oceanography 21, 285–293.

National Nuclear Data Center, 2020. https://www.nndc.bnl.gov/ensdf/. (Accessed 27 August 2020).

Nedjadi, Y., Bailat, C., Caffari, Y., Cassette, P., Bochud, F., 2015. Set-up of a new TDCR counter at IRA-METAS. Appl. Radiat. Isot. 97, 113–117.

Nedjadi, Y., Duc, P.-F., Bochud, F., Bailat, C., 2016. On the stability of ³H and ⁶³Ni Ultima Gold liquid scintillation sources. Appl. Radiat. Isot. 118, 25–31.

Nedjadi, Y., Laedermann, J.P., Bochud, F., Bailat, C., 2017. On the reverse micelle effect in liquid scintillation counting. Appl. Radiat. Isot. 125, 94–107.

Ouellet, C., Singh, B., 2011. Nuclear data sheets for A=32. Nucl. Data Sheets 112, 2199–2355.

Tan, Z., Xia, Y., 2012. Stopping power and mean free path for low-energy electrons in ten scintillators over energy range of 20–20 000 eV. Appl. Radiat. Isot. 70, 296–300.

Tykva, R., Berg, D. (Eds.), 2004. Man-Made and Natural Radioactivity in Environmental Pollution and Radiochronology. Kluwer Academic Publishers, Dordrecht.

Veicht, M., Mihalcea, I., Cvjetinovic, Đ., Schumann, D., 2021. Radiochemical separation and purification of non-carrier-added silicon-32. Radiochim. Acta 109, 735–741.

Veicht, 2022. 'Towards Implementing New Isotopes for Environmental Research: Redetermination of the ³²Si Half-Life', PhD Thesis. EPFL and PSI.